Studying the performance of solid/perforated pin-fin heat sinks using entropy generation minimization

Mohamed L. Elsayed · Osama Mesalhy

Abstract Heat transfer and pressure drop characteristics of a set of pin-fins with uniform heat flux were investigated experimentally and numerically. Test set-up was designed to assess the effects of mass flow rate, fin height, and fin density on convection heat transfer and pressure drop. In the numerical investigation, the flow field of various design parameters of the heat sink was simulated. It was found that heat sinks having fin heights of 20 and 30 mm operated at a lower Reynolds number reached minimum value for thermal resistance when the fin density 10×10. Which means it is the optimum number of fins for this case. Also, friction factor increased with a decrease in the bypass flow area or inter-fin distance spacing and using perforated fins reduced the pressure losses and thermal resistance for all studied cases.

List of symbols

D_{hd}	Duct hydraulic diameter (m)
E	Total energy per unit mass (J/kg)
H	Fin height (m)
L	Heat sink foot print length (m)
N	Number of fins
P_1	Channel inlet pressure (N/m^2)
P_L	Non-dimensional pitch $= (a + b)/a$
Q	Heat input (W)
R_{th}	Total thermal resistance (K/W)

Re_D	Reynolds number using D_h
V_d	Duct velocity (m/s)
S_g	Entropy generation minimization
h	Heat transfer coefficient (W/m^2 K)
b	Fin spacing (m)
a	Fin side thickness (m)
y^+	Dimensionless wall distance

Greek symbols

ε	Turbulent dissipation rate (m^2/s^5)
μ	Absolute viscosity (Pa s)
β	Open area ratio (%)
ρ	Density (kg/m^5)
ΔP	Pressure drop across heat sink (N/m^2)

Subscripts

B	Base plate
D_h	Hydraulic diameter

1 Introduction

The performance of many engineering devices from power electronics to gas turbines is limited by thermal management. Heat sinks with pin-fins are commonly used to augment heat transfer as the pin-fins increase the surface area and turbulence. Also, the continuing increase of power density in microelectronics and the simultaneous drive to reduce the size and weight of electronic products has led to the increased importance of thermal management issues in this industry. The temperature at the junction of an electronics package (chip temperature) has become the limiting factor determining the lifetime of a package.

Several studies have been conducted on heat sink design aimed at improving the cooling of electronic components,

M. L. Elsayed (✉) · O. Mesalhy
Mechanical Power Engineering Department, Zagazig University, Ash Sharqiyah 44519, Egypt
e-mail: mec_moh86@yahoo.com

M. L. Elsayed
Department of Mechanical and Aerospace Engineering, University of Central Florida, Orlando FL 32816-2450, USA

resulting in improved performance. Pin-fins are often used in heat exchangers as very effective elements to enhance heat transfer. The competitive ability of pin-fins compared with other high-performance fins was first investigated by Kays [1]. A similar conclusion was also reached by Kays et al. [2], while analyzing the methods for obtaining high-performance heat transfer surfaces.

The heat transfer behaviors of pin-fins have also been of interest to designers of turbine-cooling systems because of their potentially high heat transfer characteristics and surface area density, as well as their structural and castability attributes [3]. For example, in air-cooled turbine blades, such heat exchangers have made it possible for the blades to be operated at high cycle temperatures, resulting in high specific-power being achieved by modern gas turbines. A review of heat transfer and fluid flow data for arrays of pin-fins in turbine-cooling applications together with appropriate design recommendations is available in [4]. The effect of heat sink dimensions and fin density on its thermal performance was studied by Azar and Tavassoli [5]. They reported that the selection of heat sink depends not only on its thermal resistance, but also on the number of fins it has and how it is coupled to the board. There have been many investigations of the heat transfer and pressure drop of channels with pin-fins, which are restricted to pin-fins with circular cross-section and [6, 7] were among the first to investigate the heat transfer performance of in-line and staggered wall attached arrays of cylindrical fins. Several investigation on the heat transfer characteristics of staggered and inline arrays of cylindrical pin-fins done by Metzger et al. [8], Simoneau and VanFossen Jr [9] and VanFossen et al. [10].

Experiments on drop-shaped pin-fins was conducted [11]. They reported a slight enhancement of heat transfer coefficient with a remarkable 42–51 % reduction of pressure drop. Recently, Sahiti et al. [12] numerically examined six pin shapes, namely NACA, drop form, lancet, elliptic, circular, and square. Their simulation showed the NACA profile offers little advantage. Encompassing the constraints of the same hydraulic diameter, coverage ratio, and pin length, circular pin-fins, arranged in-line, still outperform other configurations. Also, a rectangular channel equipped arrays of diamond shaped elements was investigated by Tanda [13]. Both in-line and staggered fin arrays were considered in the thermal performance analysis under constant mass flow rate and constant pumping power constraints. The heat transfer performance of arrays of cubic and diamond shaped fins inside a rectangular channel was reported by Chyu et al. [14]. Convective heat transfer and friction characteristics of staggered pin-fin, triangular fin and in-line, square pin-fins arrays was performed [15, 16].

A new design criterion which involves both the effects of heat transfer performance and pressure drop was used by Boesmans et al. [17] on heat sinks of different geometries.

They found that, when pressure drop is taken into account, plate fin heat sinks have better cooling performance than offset-strip fin or pin-fin heat sinks. Kondo et al. [18] considered two types of heat sink: plate fins and pin-fins. They optimized heat sink geometry by evaluating sixteen parameters simultaneously. For the plate fins, the optimal thickness was found to be 0.12–0.15 mm. For the pin-fins, optimal pin diameters were 0.39–0.40 mm. Under the conditions of constant pumping power, the optimal thermal resistance of the plate fins was about 60 % of the pin-fins. An experimental and modeling study performed by Dogruoz et al. [19] on square, in-line pin-fin heat sinks to measure the overall thermal resistance as a function of Reynolds number and by-pass height and identify optimum pin spacing as a function of clearance ratio. Entropy generation minimization (EGM) procedure was used to optimize the overall performance of pin-fin heat sinks [20]. They showed that the entropy generation rate depends on two main performance parameters, i.e. thermal resistance and pressure drop, which in turn depend on the average heat transfer and friction coefficients.

Recently, Shaeri and Yaghoubi [21] numerically studied perforated fins, which performed better and weighed less than solid fins. Mei et al. [22] investigated by computational fluid dynamics (CFD) the effect of tip clearance on the performance of the heat transfer and pressure drop at low Reynolds number of micro-reactors with micro-pin-fin arrays (MPFAR). They found that the performance is quite sensitive to the tip clearance, and the introduced tip clearance can enhance the heat transfer and reduce the pressure drop effectively [23]. Performed Numerical computations using finite element based software COM-SOL Multiphysics around extended surfaces having various types of lateral perforations with square, circular, triangular and hexagonal cross-sections Using Reynolds-averaged Navier–Stokes (RANS) based modified k–ω turbulence model. They observed that hexagonal perforated fins show the highest fin effectiveness and the highest heat transfer performance enhancement. Also, they fond that triangular perforated fins have lowest skin friction coefficient value than the other types of fins considered.

Using Reynolds Normalized Group (RNG) based k–ε turbulent model to improve the cooling performance of solid and perforated fins that are mounted on a flat plate a three dimensional (3D) numerical study was conducted [24]. Perforations was such as small channels of square and circular cross sections are arranged along with stream wise fin's length. They found that the fins of circular perforations have remarkable heat transfer enhancement and reduced pressure drop. The review shows that the performance of the heat sink in a cross-flow is influenced remarkably by the flow velocity and the geometry of the perforation in heat sink based on [24] results. So, this work aims at investigating experimentally and numerically the

effectiveness of using different pin-fin arrangements to decrease the bypass effect. In addition to that evaluation of the thermal and hydraulic performance of the circular perforation in rectangular pin-fin by changing the Reynolds number, number of fins, and fin height.

2 Experimental investigation

2.1 Experimental set-up

Figure 1 shows the general layout of the experimental set-up used. The test rig was composed basically from a wind tunnel operated in discharge mode as indicated by the arrows, known as an open-loop suction-type. A wooden test section was mounted in the rear of the wind tunnel where the base heater and pin-fin heat sink were mounted. To describe operation of the test rig, first consider the centrifugal blower as the starting point where the flow first passes through the supply duct equipped with an orifice plate or flow straightener, before flowing through the test section. At the end, the flow was driven to the Laboratory room. The inlet velocities ranged from 1 m/s up to 20 m/s. This provides Reynolds number range of $15{,}900 < Re_D < 25{,}200$. The supply duct runs from the blower discharge to the inlet of the straightener. This duct consists of a U-shaped circular pipe of 75 mm inner diameter connected to the blower exit via a conical diffuser

(150 mm long with 5° cone angle). The other end of the U-shape is connected to the straightener via a conical nozzle (100 mm long with 12.5° cone angle). The straightener is 1.0 m long and consists of a diffuser, a settling length and a contraction. It is fitted with a honeycomb and mesh screen to ensure a uniform, low-turbulence flow from the inlet to the test channel.

2.2 Test section configuration

The general layout of the test section that contained the pin-fin array is shown in Fig. 2. The test section is 500 mm long horizontal duct of rectangular cross section 40 mm high and 150 mm wide having walls made of 5 mm Plexiglas (k = 0.2 W/m K) plates. An opening with dimensions (150 mm × 150 mm) at a distance 200 mm from the starting point of the test section was created in the bottom surface where the heater assembly is fixed. The inlet temperature of the air stream was taken as the average reading over four thermocouples located at the entrance of the test section. For the measurement of static pressures, pressure taps were made on the upper surface of the test section along the mid-span line of the heat transfer surface.

2.3 Heater block assembly

Figure 2 shows details of the heating unit consisting of the main heater, the heating surface, and insulation. The main
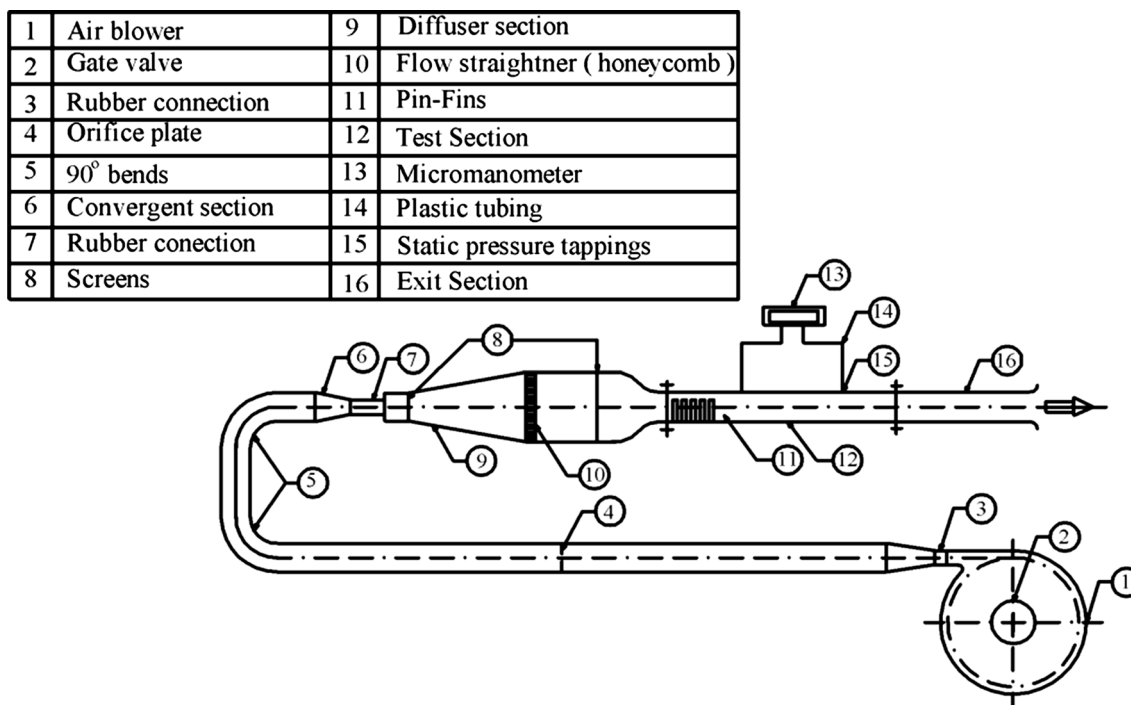
1	Air blower	9	Diffuser section
2	Gate valve	10	Flow straightner (honeycomb)
3	Rubber connection	11	Pin-Fins
4	Orifice plate	12	Test Section
5	90° bends	13	Micromanometer
6	Convergent section	14	Plastic tubing
7	Rubber conection	15	Static pressure tappings
8	Screens	16	Exit Section

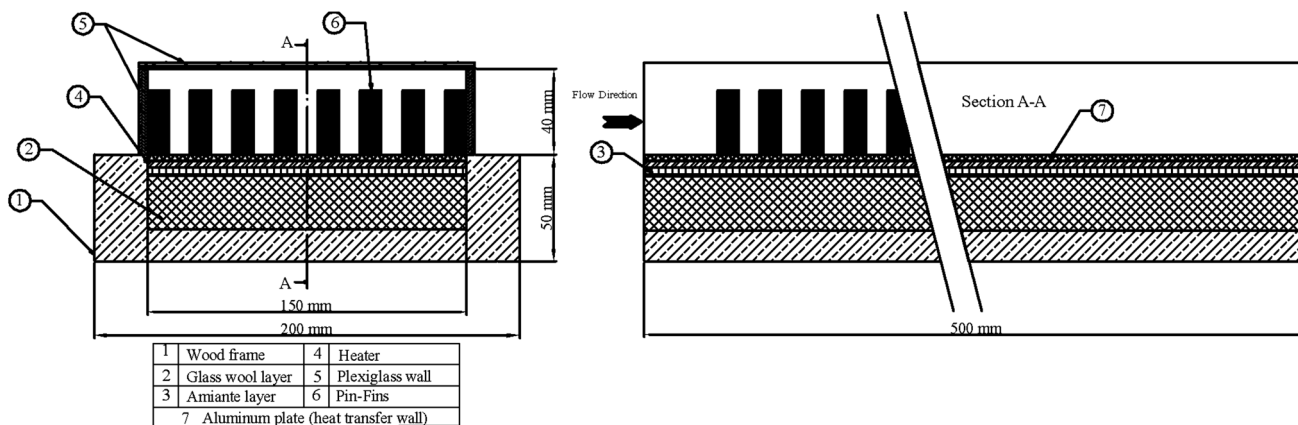**Fig. 1** Front view of wind tunnel configuration

Fig. 2 Details of heating unit

heater, a nickel–chromium resistance tape (0.2 mm thick, and 3 mm wide), heats the back surface of the aluminum plate (150 mm × 150 mm) by ohmic dissipation. The heater tape is wound uniformly around a mica board, and then embedded between another two mica boards. The insulation system placed at the bottom and sides of the heater plate consists of a 3 mm thick amiant layer (k = 0.35 W/m K) followed by a 25 mm thick glass wool layer (k = 0.041 W/m K) followed by a 20 mm thick wood board (k = 0.097 W/m K). The heat loss was estimated by measuring the temperature across the insulation substrate. The total power was measured using a DW6060 Wattmeter of range 2 kW and accuracy ±1.5 % of full scale. It was found that the maximum value of heat loss from the sides and the bottom of the heater plate was about 6 % of the total power. The heater was controlled by a variac transformer to obtain a constant heat flux along the heat transfer plate.

2.4 Pin-fin heat sink (tested models)

The configurations and detailed dimensions of the heat sink models are given in Table 1, and illustrated in Fig. 3. Using a CNC milling machine, the pin-fins were fabricated from aluminum alloy 2017, which has a thermal conductivity of (k = 202 W/m K). Experiments were conducted on pin arrays of 4 × 4, 5 × 5, 6 × 6, 7 × 7 and 8 × 8. Pins in the form of aluminum rods of rectangular cross section (10 mm × 10 mm), and height H = 20, 30, and 40 mm were distributed along the heat transfer wall at a varied pitch as in Table 1. Also, the Perforated Heat Sink was tested with open area ratio β = 15, 25, and 35 % as shown in Fig. 3. The heat sinks were mounted at the bottom of the wind tunnel duct in such a way that the pin-fin with its base was flush with the tunnel surface. It was also firmly bolted to the heater plates with a thin layer of thermal grease

Table 1 Geometric description of the tested heat sinks

Desc.	a (cm)	b (cm)	H (cm)	N	$P_L = \frac{a+b}{a}$ (cm)	A–$A_{frontal}$ (cm^2)
1A	1	1	4	8 × 8	2	28
2A	1	1.33	4	7 × 7	2.333	32
3A	1	1.8	4	6 × 6	2.8	36
4A	1	2.5	4	5 × 5	3.5	40
5A	1	3.667	4	4 × 4	4.666	44
1B	1	1	3	8 × 8	2	36
2B	1	1.33	3	7 × 7	2.333	39
3B	1	1.8	3	6 × 6	2.8	42
4B	1	2.5	3	5 × 5	3.5	45
5B	1	3.667	3	4 × 4	4.666	48
1C	1	1	2	8 × 8	2	44
2C	1	1.33	2	7 × 7	2.333	46
3C	1	1.8	2	6 × 6	2.8	48
4C	1	2.5	2	5 × 5	3.5	50
5C	1	3.667	2	4 × 4	4.666	52

having conductivity of (k = 0.7 W/m K). The base plate temperature was measured using twelve T-type thermocouples at the bottom of the heat sink base plate. Arithmetic average represents a value for the mean base plate temperature, T_b.

2.5 Data reduction

The present experimental study is divided into two parts: fluid flow and heat transfer studies. The essential quantities determined in the study of fluid flow are as follows:

Mass flow rate ($\dot{m}$) can be calculated from the measured data using an orifice meter:

$$\dot{m} = C_d \rho_a \left(\frac{\pi}{4} \frac{d_1^2 d_2^2}{\sqrt{d_1^4 - d_2^4}} \right) \sqrt{2g(\rho_f/\rho_a)\Delta h_o} \tag{1}$$
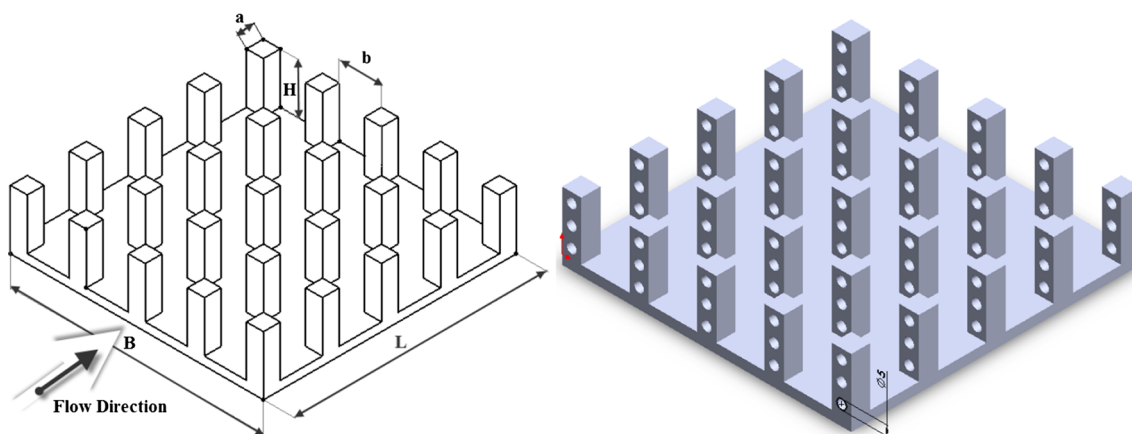
Fig. 3 Geometry of solid and perforated fin heat sink arrays

where, C_d = discharge coefficient = 0.64, ρ_a and ρ_f are the air and water (manometer fluid) density respectively, kg/m^3, g = gravitational acceleration = 9.81 (m/s^2), Δh_o = pressure head across the orifice (m H$_2$O), d_1 = diameter of supply pipe (75 mm), and d_2 = diameter of orifice (40 mm).

The Reynolds number based on approach velocity is given by:

$$Re_D = \frac{VD_h}{v} \tag{2}$$

where D_h is the hydraulic diameter of the test channel cross section:

$$D_h = \frac{4A}{P} = 0.06315 \text{ m}$$

The friction factor (f) is given by:

$$f = \frac{\Delta P}{0.5\rho V^2 \frac{L}{D}} \tag{3}$$

where, Δp = pressure drop ($P_1 - P_2$) [N/m^2], L is the measured distance between P_1 and P_2.

The heat loss to surrounding (Q_{loss}) is:

$$Q_{loss} = \frac{AK_{ins}}{\Delta X} * \Delta T_{ins} \tag{4}$$

where, A = heat sink base area (=0.0225 m^2), k_{ins} = thermal conductivity of insulation material (glass wool = 0.041 W/m K), ΔT_{ins} = temperature difference across glass wool [°C], ΔX = thickness of glass wool (ΔX = 0.025 m).

The heat transfer by convection to the air in the test channel (Q_{conv}) is:

$$Q_{conv} = Q_{tot} - Q_{loss} \text{ [W]} \tag{5}$$

Heat transfer coefficient h is given by:

$$h = \frac{Q_{conv}}{A(T_b - T_a)} \tag{6}$$

where, T_b is the local wall temperature (from thermocouple reading) [°C].

Nusselt number Nu is defined as:

$$Nu = \frac{hD_h}{K_f} \tag{7}$$

In evaluating the thermal performance of the heat sink, the thermal resistance is defined as:

$$R_{th} = \frac{T_b - T_a}{Q_{conv}} \tag{8}$$

Entropy Generation due to heat transfer and flow pressure drop is defined as [20]:

$$\dot{S}_g = \frac{Q^2 R_{th}}{T_a T_b} + \frac{\dot{m}\Delta P}{\rho T_a} \tag{9}$$

For perforated fins, the open area ratio is defined as:

$$\beta = \frac{\frac{\pi}{4}d^2 N}{aH} \tag{10}$$

where d and N are the diameter and number of holes, respectively.

The experimental uncertainties in ΔP, R_{th}, h, and Nu were the result of uncertainties in the experimental measurement of temperature, pressure, flow rate, power, and uncertainty in the thermal and fluid properties of the cooling fluid. The result of that analysis is summarized in Table 2.

3 Numerical investigation

3.1 Problem description and boundary condition

The geometry of the theoretical model and the boundary conditions are illustrated in Fig. 4 which shows the physical domain of the channel and the pin-fin heat sink. The

Table 2 Uncertainties in compound variables

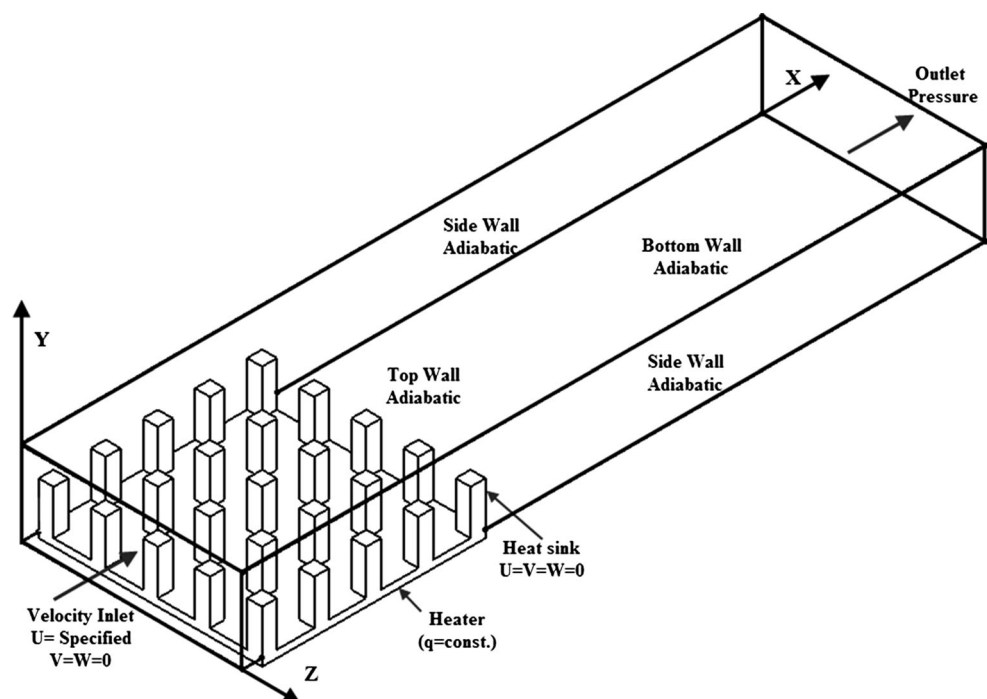| Compound variable	Uncertainty (± %)
Mass flow rate (kg/s)	1.84
Friction factor	4.97
Reynolds number	1.84
Thermal resistance	1.5
Convective heat transfer coefficient	1.5
Nusselt number	1.5

thermal and flow fields were calculated numerically with commercial CFD software ANSYS FLUENT 13, according to the following assumptions: the flow was steady state; the flow was incompressible and turbulent; the fluid and the solid properties were constant, and the effects of gravitation and thermal radiation were neglected. The equations governing the fluid are the Reynolds-averaged Navier–Stokes equations and the energy equation. Based on the aforementioned assumptions these equations can be expressed as:

$$\frac{\partial}{\partial x_i}(\rho V_i) = 0.0 \tag{11}$$

$$\frac{\partial}{\partial x_i}\left(\rho V_i V_j\right) = -\frac{\partial P}{\partial x_i} + \frac{\partial \tau_{ij}}{\partial x_j} \tag{12}$$

$$\frac{\partial}{\partial x_i}[V_i(\rho E + P)] = \frac{\partial}{\partial x_i}\left(K\frac{\partial T}{\partial x_i}\right) \tag{13}$$

where, i: is a tensor indicating 1, 2, and 3 and τ_{ij} is the viscous stress tensor.

RNG κ–ε turbulent model was utilized [24] to solve the complicated turbulent thermal flow field with Enhanced Wall Function approach in the near-wall regions to fit the wall boundary conditions [25]. The solid regions, fins and the heat sink base, were also considered, where only the heat diffusion equation is solved. The solution was considered converged when the scaled residual of the energy equation reached 10^{-7} and the scaled residuals of other equations reached 10^{-4}.

3.2 Mesh generation and discretization

The geometry and mesh of the computational model were generated separately using GAMBIT 2.4.6. The Hex/Sub Mapped and Hex/wedge Cooper meshing scheme was used to refine the mesh near walls and beside sharp edges. To test the dependence of the numerical results on the grid density, calculations were carried out with different mesh densities in the X, Y and Z directions. As recommended by Fluent Guide AFUs [25], the first grid points adjacent to the walls were kept at y^+ values between 1 and 5. The applied grid system was certified under conditions of a heat sink with a 6 × 6 fin array, H = 30 mm, and Re = 22,500. The grid sensitivity was analyzed mainly to obtain grid independent temperature distributions. The computational results of the mean surface temperature of the heat sink did not show a variation more than 0.04 % in thermal resistance when the grid size increased from 320,230 to 570,900. It is clear that the effect of grid size on the computed result diminishes for grids of 320,230 nodes.

Fig. 4 Boundary conditions for channel with fins

4 Results and discussion

4.1 Pin-fin effects on velocity and flowfields

Attaching rectangular pin-fins to the heater base plate is expected to make a drastic change to the velocity and temperature fields. So, to better understand the effect on thermal performance, the flow and temperature fields will be illustrated first for a selected heat sink design as shown in Table 3.

Figure 5 shows the flow streamlines and pressure contours in the horizontal plane passing at the mid height of the test section as well as in the vertical plane passing through the fins. As shown from the streamlines in the horizontal plane, the presence of the fins generates vortices downstream of each row. This in turn generate turbulence and enhance the heat transfer rate. The main flow streamlines in the fin region flow through the lanes between the fins. The streamlines in the vertical plane show that the flow accelerates as it enters the bypass region. A considerable part of the flow rate passes through the bypass region and the remaining part that performs the forced convection passes through the space between the fins. When the pin-fin height increases (no tip clearance), the blockage effect of the fins increases, forcing more coolant fluid to pass through the heat sink. So, it is expected that for the case of no bypass flow, an advantage of enhancing the heat transfer from the heat sink is gained. The pressure contours show that due to the blockage effect of the heat sink, the pressure evidently increases upstream in front of the heat sink. As the fluid enters the heat sink, the pressure decreases gradually with the distance due to the viscous friction and wake formation. After the flow leaves the heat sink the pressure recovers again due to the increase in the area of the test section.

The calculated thermal resistance and friction factor at different Reynolds numbers are shown in Fig. 6. In general, the thermal resistance decreases substantially and diminishes smoothly with an increase in the Reynolds number. But the pressure drop across the heat sink increases dramatically as the Reynold's number increases,
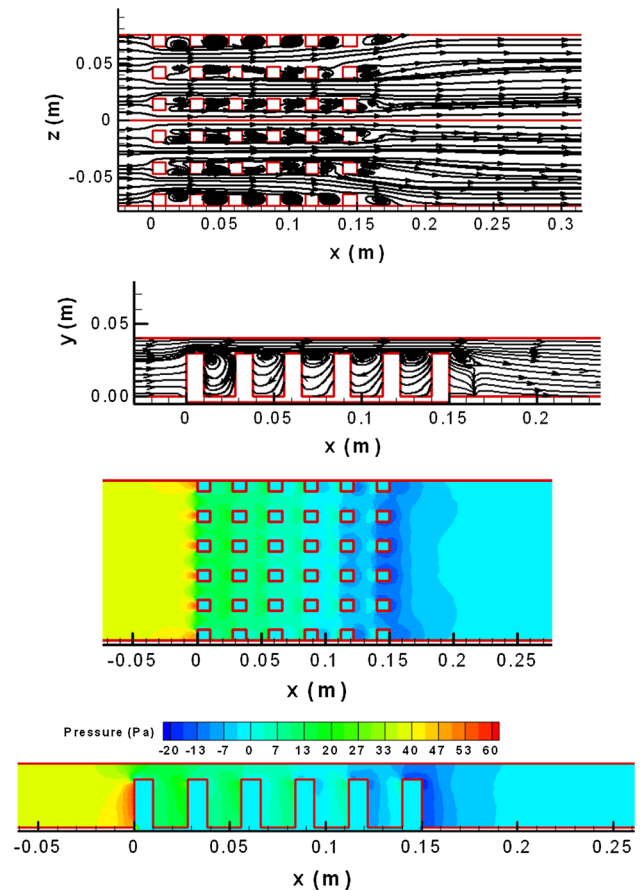

Fig. 5 Streamlines and pressure contours at a mid *horizontal plane* and a *vertical plane* passing through the fins

due to the presence of pin-fins, while the friction factor decreases. Thermal resistance decreases to almost half its value without too much increase in pressure drop and consequently the pumping power. The figures also show a comparison between the measured and the predicted values, showing good agreement in both magnitude and trend of the data.

4.2 Parametric study

In order to identify and assess the impact of the design parameters, a parametric study was carried out to check the effect of changing the design parameters on the performance of the heat sink. These design parameters have been identified as, Reynolds Number Re_{Dh}, fin height H, and density. Table 4 shows the range of these parameters. Fifteen pin-fin heat sinks were used in this study.

4.2.1 Effect of Reynolds number at different fin heights

Figure 7 shows the effect of Reynolds number on the thermal performance of the heat sink. As expected, the thermal
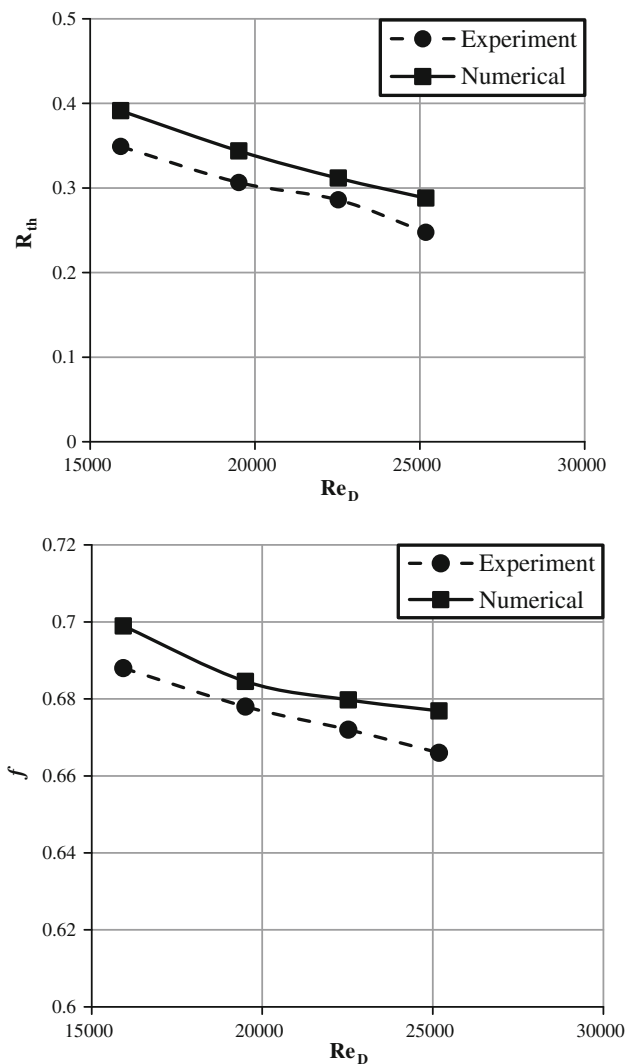
Table 3 Values of parameters considered in base case (3B)

Parameter	Value
Air inlet temp. (°C)	27
Heat input (W)	30
Fluid velocity (m/s)	3.8
Heat sink dimension	
Fin height H	30 mm
Fin number N	6
Fin side length a	10 mm
Fin spacing b	18 mm

Fig. 6 Effect of Reynolds number on thermal resistance and friction factor for 3B heat sink

Table 4 Values of test matrix parameters

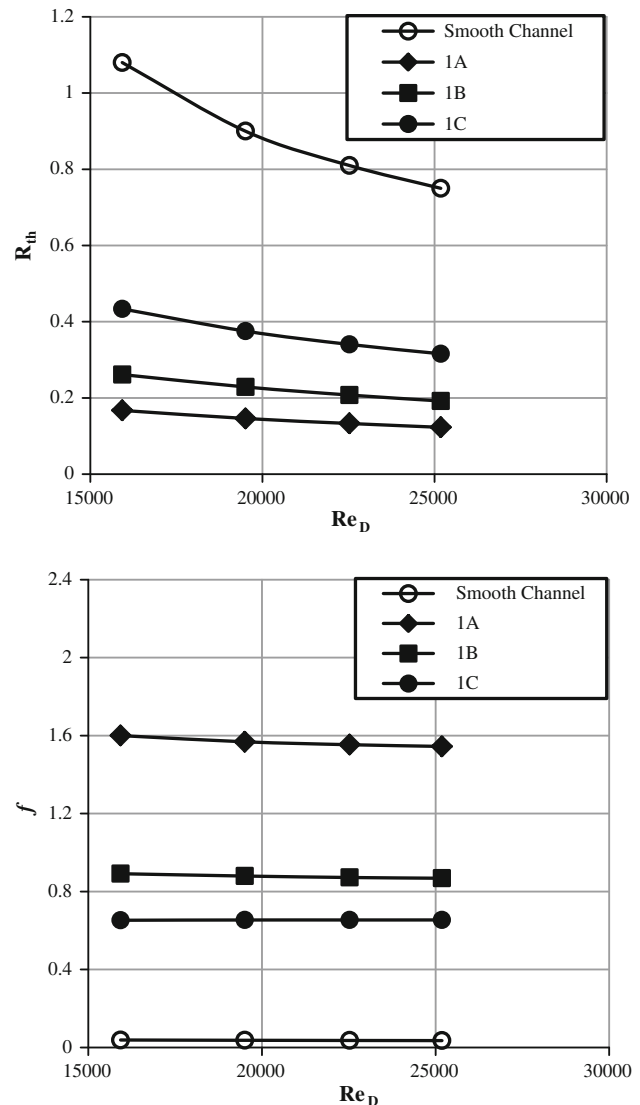| Parameter	Value
Air inlet temperature (°C)	27
Heat input (W)	30
Fluid velocity (m/s)	3.8, 5, 6, and 7 m/s
Fin height H	20, 30, 40 mm
Fin numbers N	4, 5, 6, 7, 8, 9, 10, 11

Fig. 7 Effect of fin height on thermal resistance and friction factor for different Reynolds numbers

resistance decreases with an increase in both the Reynolds number and fin height. Increasing the Reynolds number increases the cooling effect while increasing fin height increases the surface area. Installing pin-fins improves the thermal performance through reducing the heat sink's thermal resistance especially for the case of lower Reynolds number. As the heat sink height increases, the improvement in thermal resistance slightly decreases. The pressure drop across the pin-fin heat sink is due to two components namely, skin friction and form drag. Skin friction is responsible for almost all the pressure drop at low Reynolds number. As the Reynolds number increases, the contribution of skin friction to form drag decreases. Also, Fig. 7 shows the variation of the friction factor with the Reynolds number. The pressure drop is relatively small without the pin-fins and it increases gradually with the Reynolds number and with heat sink height. This is attributed to the higher skin friction and form

drag associated with increasing the Reynolds number and heat sink height, respectively.

4.2.2 Effect of fin numbers

Figure 8 Shows the effect of pin-fin numbers at various Reynolds number with constant fin height H = 40 mm on
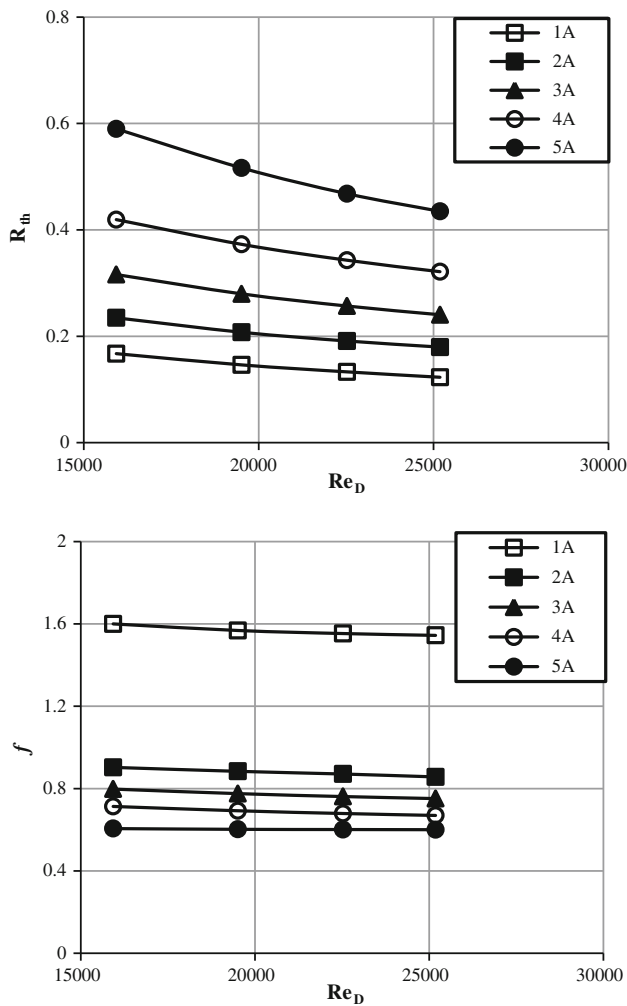
Fig. 8 Effect of number of fins on thermal resistance and friction factor for H = 40 mm

Fig. 9 Distribution of thermal resistance pressure coefficient with dimensional pitch length for Re_D = 15,927

the thermal resistance. The figure shows that the thermal resistance of the heat sink decreases generally with an increase in the Reynolds number. Using a heat sink with larger fin height or operating the heat sink at a higher Reynolds number causes the heat sink to attain minimum thermal resistance with a higher number of fins. Also, it shows the effect of the number of fins at various Reynolds number with constant fin height H = 40 mm on the pressure drop across the heat sink. It is clear that the pressure drop increases as the number of fins increases for all cases.

4.3 Optimization of thermal resistance

One of the goals of this study was to predict the optimal number of pin-fins and design configurations that would maximize the heat transfer rate while minimizing frictional losses in the flow. A parametric optimization was performed on pin-fin heat sinks, at various fin heights with a constant Reynolds number Re_D = 15,927. Figure 9 shows
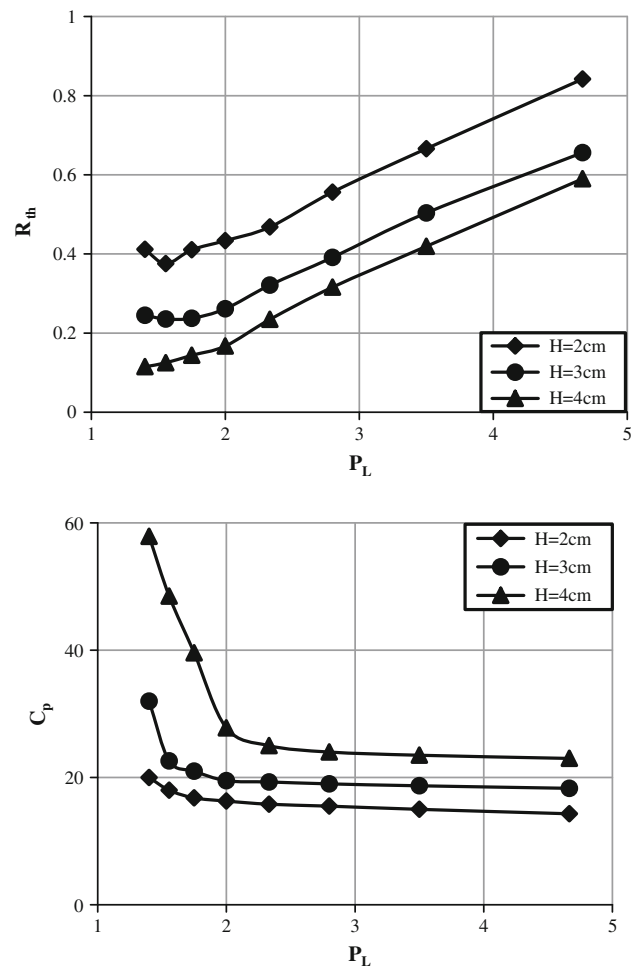
the effect of the number of pin-fins on thermal resistance using Dimensionless Pitch (P_L). It is clear that increasing the number of fins (P_L decreases), thermal resistance decrease in case of fins height H = 40 mm without limit but in the case of fin height H = (30 and 20 mm) thermal resistance decrease and then increase so there is an optimum fins spacing, and this is due to effect of by-pass in case of fins height of 30 and 20 mm. For H = 20 and 30 mm, the thermal resistance reached its minimum value at P_L = 1.5, and N = 10 which means that this number of fins is the optimum for a heat sink with H = 20 mm, operating at Re = 15,927. This optimum operating point occurs because of the two contradicting effects caused by increasing the number of fins. These effects consist of increasing the heat transfer surface area and increasing the blockage effect. Using a heat sink with larger fin height or operating the heat sink at a higher Reynolds number causes the heat sink to attain minimum thermal resistance at a higher number of fins. The figure also shows that increasing fin height eliminates this optimum point (N = 10 at
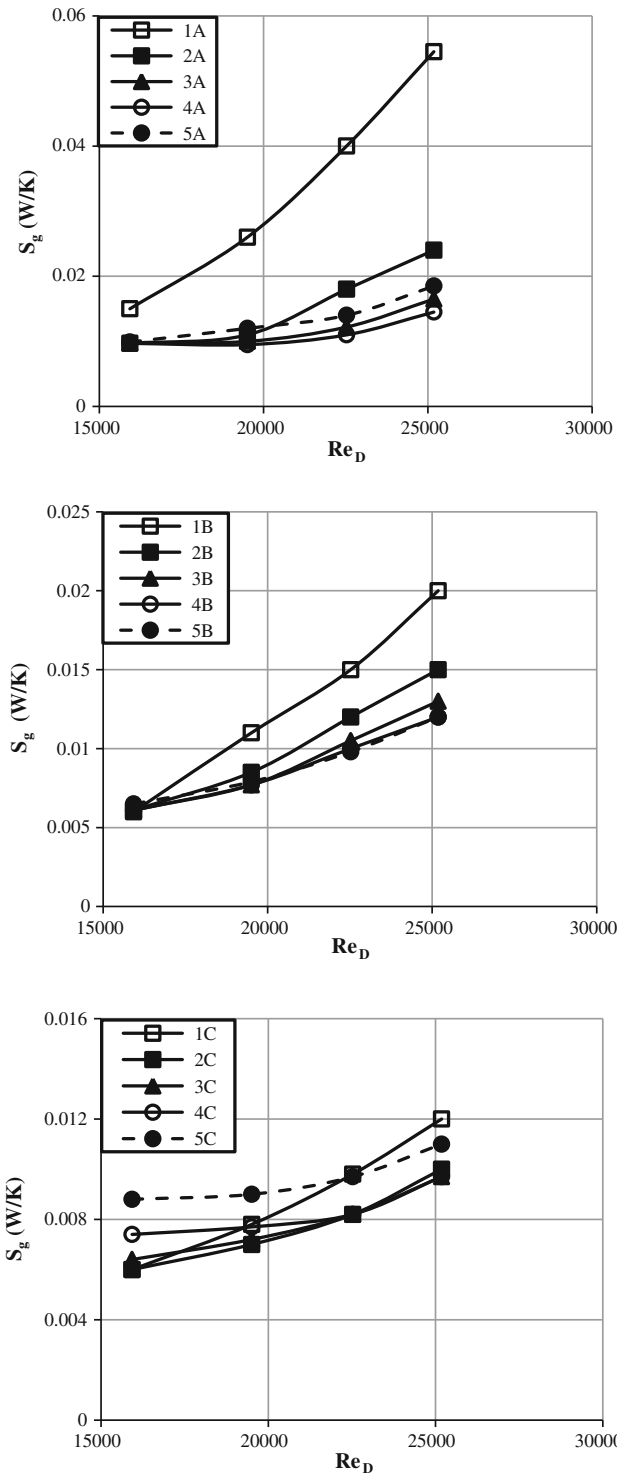
Fig. 10 Variation of S_g with Re_D for heat sink with different number of fins and fin heights

Fig. 11 Effect of open area ratio on thermal resistance and friction factor for 5A perforated heat sink

Re = 15,927), which means that decreasing the bypass area makes it possible to increase the number of fins to gain more improvement in the thermal performance. Also, Fig. 9 shows the effect of fin height and fin spacing on the pressure coefficient. Increasing fin height and the number
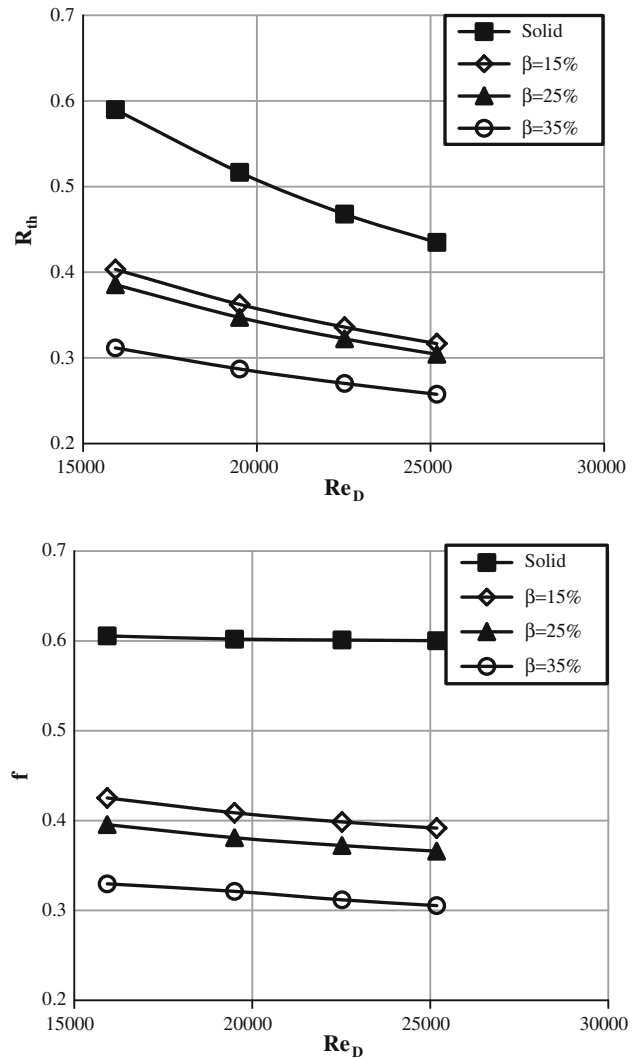
of fins increases the pressure drop but this decreases thermal resistance too.

Another way to study the optimization is to use entropy generation minimization procedure which is employed to optimize the overall performance (thermal and hydrodynamic) of pin-fin heat sinks. This allows the combined effects of thermal resistance and pressure drop to be assessed simultaneously as the heat sink interacts with the surrounding flow field. The formulation for the dimensionless entropy generation rate is obtained in terms of fin geometry, longitudinal and transverse pitches, pin-fin aspect ratio, thermal conductivity, arrangement of pin-fins, Reynolds and Prandtl numbers. It is shown that the entropy generation rate depends on two main performance parameters, i.e. thermal resistance and the pressure drop, which in turn depend on the average heat transfer and friction coefficients. These coefficients can be taken from fluid flow
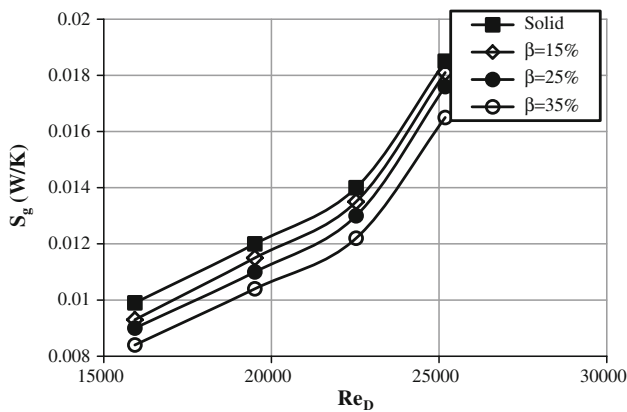
Fig. 12 Variation of S_g with Re_D for 5A perforated heat sink

and heat transfer models. Figure 10 shows the effect of increasing Reynolds number on EGM for a heat sink with fin height H = 40, 30 and 20 mm respectively and for various fin spacing, Although, heat sinks 1A and 1B have the lowest thermal resistance, and their pressure drop is the highest So, it has the highest entropy generation. But for a low Reynolds number, nearly all the heat sinks have the same EGM. Also, heat sink 1C has the lowest thermal resistance and high pressure drop, giving it the highest EGM for high $Re_D = 25,200$, but heat sink 5C has high EGM because it has high thermal resistance. Also, heat sinks with more fins have the lowest performance especially with taller fins or operating at a higher Reynold's number. However, heat sinks with shorter fins operate better for lower Reynold's number and fewer fins.

4.4 Peforated fins

Figure 11 shows the effect of fin perforation (perforation ratio β = 15, 25 and 35 %) of the pin-fin heat sinks, at various Reynolds numbers with constant fin height H = 40 mm and fin number N = 4, on the thermal resistance and pressure drop. It shows that the thermal resistance of the heat sink decreases generally with an increase in the open area ratio and it is clear that the pressure drop for solid fins is higher than for perforated fins and the friction factor decreases as the open area ratio increases. Finally, Fig. 12 shows the effect on entropy generation of increasing the open area ratio for heat sinks with a fin height H = 40 mm and for various Reynolds numbers. It is clear that solid fins have highest EGM since the pressure drop and thermal resistance is high and EGM decreases as the open area ratio β increases and the lowest value of EGM for this case was β = 35 %. However, the optimum point is not seen in the covered range of open area ratio to be taken as the optimum open area ratio for the array.

5 Conclusions

The thermal performance of pin-fin heat sinks undergoing cross-flow cooling has been studied experimentally and numerically and the following conclusions have been drawn.

- In the case of no by-pass (case A) increasing the number of fins increases the exposed area to the flow and promotes turbulence. As there is no by-pass effect, this case shows the smallest thermal resistance but gives the highest pressure drop.
- The friction factor increases with decreasing bypass flow area and inter-fin distance spacing.
- For fin height of 20 and 30 mm, increasing the number of fins increases the exposed area to the flow and enhances turbulence so thermal resistance decreases but the by-pass effect also increases, the former increase thermal resistance and the latter decreases it so the optimum fin spacing is equal to 5 mm.
- For the same fin spacing, increasing the fin height reduces the by-pass effect, resulting in the thermal resistance decreasing and the pressure loss increasing.
- Perforated fins reduce the pressure loss and thermal resistance for cases being studied β = 15, 25 and 35 %.
- Solid fins have the highest EGM since the pressure drop and thermal resistance are high and EGM decreases as the open area ratio β increases. The lowest value of EGM for case 5A was β = 35 %.

References

1. Kays WM (1953) Pin fin heat exchanger surfaces, Department of Mechanical Engineering, Stanford University; Office of Naval Research, US
2. Kays WM, Crawford ME, Weigand B (1993) Convective heat and mass transfer. McGraw-Hill, New York
3. Peng Y (1983) Heat transfer and friction loss characteristics of pin fin cooling configuration. In: 28th international gas turbine conference and exhibit
4. Armstrong J, Winstanley D (1987) A review of staggered array pin fin heat transfer for turbine cooling applications. In: 32nd international gas turbine conference and exhibition
5. Azar K, Tavassoli B (2003) How much heat can be extracted from a heat sink? Electron Cool 9:30–37
6. Sparrow E, Ramsey J (1978) Heat transfer and pressure drop for a staggered wall-attached array of cylinders with tip clearance. Int J Heat Mass Transf 21:1369–1378
7. Sparrow E, Ramsey J, Altemani C (1980) Experiments on in-line pin fin arrays and performance comparisons with staggered arrays. J Heat Transf 102:44
8. Metzger D, Berry R, Bronson J (1982) Developing heat transfer in rectangular ducts with staggered arrays of short pin fins. J Heat Transf 104:700
9. Simoneau R, VanFossen G Jr (1984) Effect of location in an array on heat transfer to a short cylinder in crossflow. J Heat Transf 106:42–48

10. Matsumoto R, Kikkawa S, Senda M (1997) Effect of pin fin arrangement on endwall heat transfer. JSME Int J Ser B 40:142–151

11. Chen Z, Li Q, Meier D, Warnecke H-J (1997) Convective heat transfer and pressure loss in rectangular ducts with drop-shaped pin fins. Heat Mass Transf 33:219–224

12. Sahiti N, Lemouedda A, Stojkovic D, Durst F, Franz E (2006) Performance comparison of pin fin in-duct flow arrays with various pin cross-sections. Appl Therm Eng 26:1176–1192

13. Tanda G (2001) Heat transfer and pressure drop in a rectangular channel with diamond-shaped elements. Int J Heat Mass Transf 44:3529–3541

14. Chyu M, Hsing Y, Natarajan V (1998) Convective heat transfer of cubic fin arrays in a narrow channel. J Turbomach 120:362–367

15. Al-Jamal K, Khashashneh H (1998) Experimental investigation in heat transfer of triangular and pin fin arrays. Heat Mass Transf 34:159–162

16. Şara O, Yapıcı S, Yılmaz M, Pekdemir T (2001) Second law analysis of rectangular channels with square pin-fins. Int Commun Heat Mass Transf 28:617–630

17. Boesmans B, Christiaens F, Berghmans J, Beyne E (1994) Design of an optimal heat-sink geometry for forced convection air cooling of Multi-Chip Modules. In: Thermal management of electronic systems. Springer, Berlin, pp 267–276

18. Kondo Y, Matsushima H, Komatsu T (2000) Optimization of pin-fin heat sinks for impingement cooling of electronic packages. J Electron Packag 122:240

19. Dogruoz MB, Urdaneta M, Ortega A (2005) Experiments and modeling of the hydraulic resistance and heat transfer of in-line square pin fin heat sinks with top by-pass flow. Int J Heat Mass Transf 48:5058–5071

20. Khan WA, Yovanovich M, Culham J (2006) Optimization of microchannel heat sinks using entropy generation minimization method. In: Semiconductor thermal measurement and management symposium, 2006 IEEE twenty-second annual IEEE IEEE, pp 78–86

21. Shaeri M, Yaghoubi M (2009) Thermal enhancement from heat sinks by using perforated fins. Energy Convers Manag 50:1264–1270

22. Mei D, Lou X, Qian M, Yao Z, Liang L, Chen Z (2014) Effect of tip clearance on the heat transfer and pressure drop performance in the micro-reactor with micro-pin-fin arrays at low Reynolds number. Int J Heat Mass Transf 70:709–718

23. Ismail MF, Hasan MN, Saha SC (2014) Numerical study of turbulent fluid flow and heat transfer in lateral perforated extended surfaces. Energy 64:632–639

24. Ismail MF, Reza M, Zobaer M, Ali M (2013) Numerical investigation of turbulent heat convection from solid and longitudinally perforated rectangular fins. Proced Eng 56:497–502

25. Fluent Guide AFUs (2010) Release 13.0. ANSYS. Inc, Canonsburg, PA